

Study of pressure-induced amorphization in sulfur using *ab initio* molecular dynamics

Dušan Plašienka* and Roman Martoňák

Department of Experimental Physics, Comenius University, Mlynská Dolina F2, 842 48 Bratislava, Slovakia

(Received 28 January 2012; revised manuscript received 15 March 2012; published 30 March 2012)

We report results of *ab initio* constant-pressure molecular dynamics simulations of sulfur compression leading to structural transition and pressure-induced amorphization. Starting from the orthorhombic S-I phase composed of S_8 ring molecules we find at room temperature and pressure of 20 GPa a transformation to monoclinic phase where half of the molecules develop a different conformation. Upon further compression, the monoclinic phase undergoes pressure-induced amorphization into an amorphous phase, in agreement with experiments. We study the dynamics of the amorphization transition and investigate the evolution of intra and intermolecular distances in the monoclinic phase in order to provide a microscopic insight into the rings disintegration process leading to amorphization. In the amorphous form we examine the structural properties and discuss its relation to the experimentally found amorphous form and to underlying crystal phases as well. The amorphous form we find appears to correspond to the experimentally observed low-density amorphous form.

DOI: [10.1103/PhysRevB.85.094112](https://doi.org/10.1103/PhysRevB.85.094112)

PACS number(s): 61.43.Bn, 61.43.Dq, 64.70.kg

I. INTRODUCTION

Pressure is a key external variable determining structure and properties of solids. The most dramatic effect induced by pressure are structural transformations between different crystalline phases. Providing access to number of polymorphs, pressure-induced structural transitions are of academic as well as practical interest in solid-state physics and materials science. Besides transitions between stable or metastable crystalline forms, transitions from crystal to amorphous form have been observed in various materials, such as H_2O ,¹ Si,² SiO_2 ,³ etc. The process has been called pressure-induced amorphization (PIA) and since it was first studied in compressed ice,¹ its nature as well as the character of the amorphous form created in this way has been extensively discussed (see Refs. 4 and 5 for a detailed review on this topic). Open questions include a number of issues. First is the connection of the amorphous form created in this way to liquid or crystalline phase. It was recognized that it might be structurally connected either to higher-temperature liquid phase (and its corresponding glass), or, alternatively, could represent a disordered version of some underlying crystalline phase. Another discussion concerns the mechanism of PIA and its thermodynamical description. PIA has been originally explained as metastable melting, recognizing that compressed ice amorphized upon crossing the negatively sloped melting line of water extrapolated to low temperatures.¹ Another scenario referred to as mechanical melting is based on observation that the structure collapse might be driven by elastic or lattice instabilities (by softening of certain elastic or phonon shear modes) at high pressure conditions.^{6,7} Upon approaching PIA, it has been commonly observed that the x-ray diffraction patterns become less crystalline, suggesting that creation of defects often precedes the phenomenon of PIA.

In some materials the existence of more amorphous forms that differ in density and microscopic structure has been observed. This phenomenon was called polyamorphism, analogously to polymorphism. It has been found that at least two different forms exist that have been called low-density-amorphous (LDA) and high-density-amorphous (HDA) forms.

Polyamorphism was first observed in compressed ice⁸ and since then has been experimentally and theoretically studied in a number of other common elements and compounds like Si,^{2,9} Ge,¹⁰ SiO_2 ,^{11,12} etc. While in some cases the amorphous-amorphous transition (AAT) was found to be sharp,^{8–10} in other systems it was observed to proceed gradually.^{11,13} The sharpness of the transition might also be temperature dependent, as observed, e.g., in SiO_2 , where densification is promoted at elevated temperatures in certain pressure region associated with the “reversibility window.”^{12,14} Similar to the case of PIA, it has been found that there could be a connection of AAT to liquid-liquid transition at higher temperatures or to thermodynamical crystal-crystal transformation (see Refs. 15–17 for a review on the phenomenon of AAT).

Recently, the existence of PIA as well as of polyamorphism has been reported also in sulfur.^{18–20} Sulfur is one of the most common and important elements and its crystal structure at ambient conditions belongs to the most complex ones found among pure elements. Sulfur was experimentally studied in the pressure range from 0 to 230 GPa and at least ten different stable crystal structures have been identified. A thermodynamic phase diagram of sulfur is presented in Fig. 1. The diagram is based on data from number of experiments.^{18,21–29}

The stable structure of sulfur at ambient conditions is orthorhombic structure S-I, which is highly complex as its unit cell consists of 128 atoms in 16 S_8 ring molecules. At temperatures close to melting curve, S-I transforms to S-II upon pressure increase at 1.5 GPa and if thereafter quenched to room temperature, S-II transforms further to S-III at 36 GPa.²³ The structures of S-II and S-III are similar—both are polymeric and consist of chains. S-II is trigonal and formed by molecules with the shape of triangular chains and S-III is tetragonal with square-shaped chains.^{22,23,26,33} Both structures are very different from the molecular S-I phase and, therefore, one can expect that they are separated from S-I by high-energy barriers. The complex transition mechanism between molecular and polymeric sulfur needs to include bond breaking in S_8 molecules and complete reorganization of the entire structure.

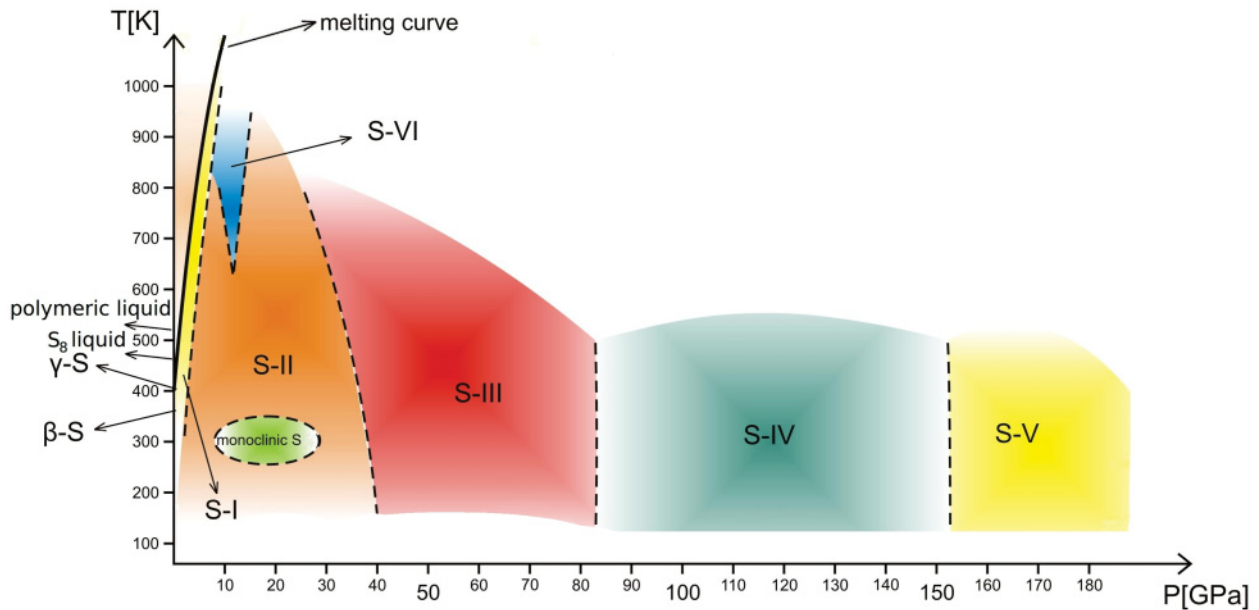


FIG. 1. (Color online) Thermodynamic phase diagram of sulfur. True thermodynamic stability regions of some phases are uncertain because large hysteresis on compression/decompression has been observed in the experiments.^{22,23} Existence of some other crystalline phases was proposed by numerical simulations.^{30–32}

At pressures over 83 GPa, S-III transforms into aperiodic incommensurately (IC) modulated monoclinic phase S-IV.^{25,27,34} Further increase of pressure above 135 GPa results into formation of phase S-V with rhombohedral β -Po structure.^{24–26,35} The high-pressure phases of sulfur exhibit different electrical properties. While low-pressure phases up to S-II are insulating, S-III is a semiconductor and S-IV and higher-pressure phases are found to be metallic and superconducting.^{29,34,36–39}

Sulfur at ambient pressure melts at 115 °C²¹ and then upon rising temperature undergoes a liquid-liquid transition at around 160 °C^{40–42} from S₈ molecular liquid to viscous polymeric liquid with rubberlike properties⁴³ that is metallic.⁴⁴ The process of ring-opening polymerization resulting into creation of helical chains was simulated in Refs. 45 and 46. By rapid quenching of this sulfur melt, an amorphous version of solid sulfur that contains polymeric chains is created. A very stable version of amorphous sulfur prepared by a rapid compression to 2 GPa has been recently reported.⁴⁷

Because of high barriers separating S-I from polymeric phases one can expect strong kinetic effects and metastability, in particular at low temperatures. Indeed, it was found that at room temperature compression of S-I results in a transformation to S-III only when pressure of 36 GPa is reached, thus completely skipping the S-II structure.²³ Metastability of the S-I molecular phase is found also in all experiments observing PIA, upon approaching the pressure of amorphization.^{18–20}

Luo and Ruoff¹⁸ compressed S-I at room temperature and found a transition to a monoclinic phase at about 5 GPa. It was, however, not possible to determine the exact structure of this phase. Upon further increase of pressure they observed a reversible amorphization starting at 18 GPa and completed at 25 GPa. Between 18 and 25 GPa they observed significant decrease in intensity and increase in width of diffraction

peaks resulting in lower number of diffraction peaks observed. Recrystallization to an unknown phase was observed at 37 GPa.³⁵ Similar results were observed in Ref. 48.

In Ref. 18, authors proposed two possible mechanisms of PIA. In the first scenario, the system attempts to transform into new structure but remains trapped in disordered state before completing the transition because of insufficient mobility of the atoms, which does not allow the reorganization of the structure. The second scenario represents amorphization triggered by intramolecular bond breaking.

Gregoryanz *et al.* (Ref. 20) studied amorphization of sulfur at room temperature and below. They also observed that diffraction reflections first start to broaden and decrease in intensity at 25 GPa between 80 and 175 K. Subsequently, PIA takes place and is completed at 47 GPa at 80 K, at 45 GPa at 175 K, and at 37 GPa at 300 K. The authors discussed the discrepancy of the amorphization pressure compared to that found in Ref. 18 and suggested it could be explained by the use of different experimental techniques. While the work of Luo and Ruoff¹⁸ was based on energy-dispersive diffraction, in Ref. 20 the more conventional angle-dispersive methods were used. Authors also pointed out that the extrapolated P-T boundary of amorphization appears to connect to the metastable extension of the high-pressure melting curve.

In addition to PIA, Ref. 19 reported the observation of LDA-HDA polyamorphic transition in sulfur above 65 GPa at temperature 40 K. According to the density and coordination number measured for these forms, authors suggested that the LDA and HDA forms might correspond to their crystalline counterparts, namely polymeric S-III and metallic S-IV. They also pointed out that there is a crossing of the S-III/S-IV phase boundary behind the LDA-HDA transition. However, they also admit the possibility that besides a genuine polyamorphism the experimental data might be as well compatible with the

creation of small nanocrystals in the sample. This cannot be distinguished from the genuine amorphous form within the resolution of the x-ray diffraction technique.

In this paper, we aim at resolving the open questions concerning the PIA and polyamorphism in sulfur by means of *ab initio* constant-pressure molecular dynamics. Both Refs. 18 and 20 indicate that before PIA the structure undergoes substantial changes. It is plausible to assume that in the conditions of strong overpressurization the S_8 molecules do not remain intact and become distorted even before the onset of PIA. Since it was not possible to determine the precise character of these structural changes experimentally, it appears useful to complement the experiments by computer simulation. This could also shed light on the microscopic mechanism of the PIA and help to understand the subsequent polyamorphic transition. The paper is organized as follows. In Sec. II we present the simulation methods. In Sec. III we describe the simulation protocol and discuss the results and compare them to experimental data. In the final section we draw some conclusions.

II. SIMULATION METHODS

To perform *ab initio* molecular dynamics (MD) simulations we used VASP package.^{49–52} To simulate system under constant pressure, we used the idea based on the Berendsen barostat.⁵³ After performing 20 MD steps with time step of 2 fs in constant supercell (total simulated time of 40 fs), we rescaled parameters of the supercell according to the difference of external pressure P_{ext} and averaged internal pressure in the system P_{int} following the Berendsen scheme. We note that our procedure is slightly different from the original one⁵³ because we do not apply the scaling at every MD step.

The cell matrix $\mathbf{h} = (\vec{a}, \vec{b}, \vec{c})$ where the three vectors $\vec{a}, \vec{b}, \vec{c}$ span the simulation supercell, together with atomic positions \mathbf{r}_i and velocities \mathbf{v}_i were transformed by the scaling matrix $\boldsymbol{\mu}$ following the rule

$$\mathbf{h} \rightarrow \boldsymbol{\mu}\mathbf{h}, \quad \mathbf{r}_i \rightarrow \boldsymbol{\mu}\mathbf{r}_i, \quad \mathbf{v}_i \rightarrow \boldsymbol{\mu}\mathbf{v}_i,$$

$$\boldsymbol{\mu} = \mathbf{1} - \frac{\beta\Delta t}{3\tau_P} (\mathbf{P}_{\text{ext}} - \mathbf{P}_{\text{int}}),$$

where β is the bulk modulus of the system, Δt is the time step of the transformation (40 fs in our case), and τ_P is the relaxation time scale defining how quickly the algorithm responds to pressure fluctuations (only the $\frac{\beta\Delta t}{3\tau_P}$ ratio is relevant).

All simulations were performed on a sample consisting of 512 atoms in a supercell (generated as $2 \times 2 \times 1$ supercell of S-I unit cell) with periodic boundary conditions. The core electrons were dealt with the projector augmented wave (PAW) pseudopotential method.^{54,55} Each atom contributed to the electronic problem with six electrons from $3s^2$ and $3p^4$ sulfur valence orbitals. These electrons were treated by means of density functional theory (DFT) within the generalized gradient approximation (GGA) in the Perdew-Burke-Ernzerhof⁵⁶ (PBE) scheme. The Kohn-Sham equations⁵⁷ were solved in a plane wave basis set with energy cutoff of 360 eV. Since the supercell was fairly large ($22 \times 27 \times 25$ Å at 0 GPa) the k -point grid was well approximated by taking only the Γ point.

III. SIMULATION RESULTS AND DISCUSSION

A. Simulation protocol

The simulation protocol together with the experimental data for amorphous sulfur from Refs. 18–20 is schematically shown on Fig. 2. We started the simulation from the optimized S-I

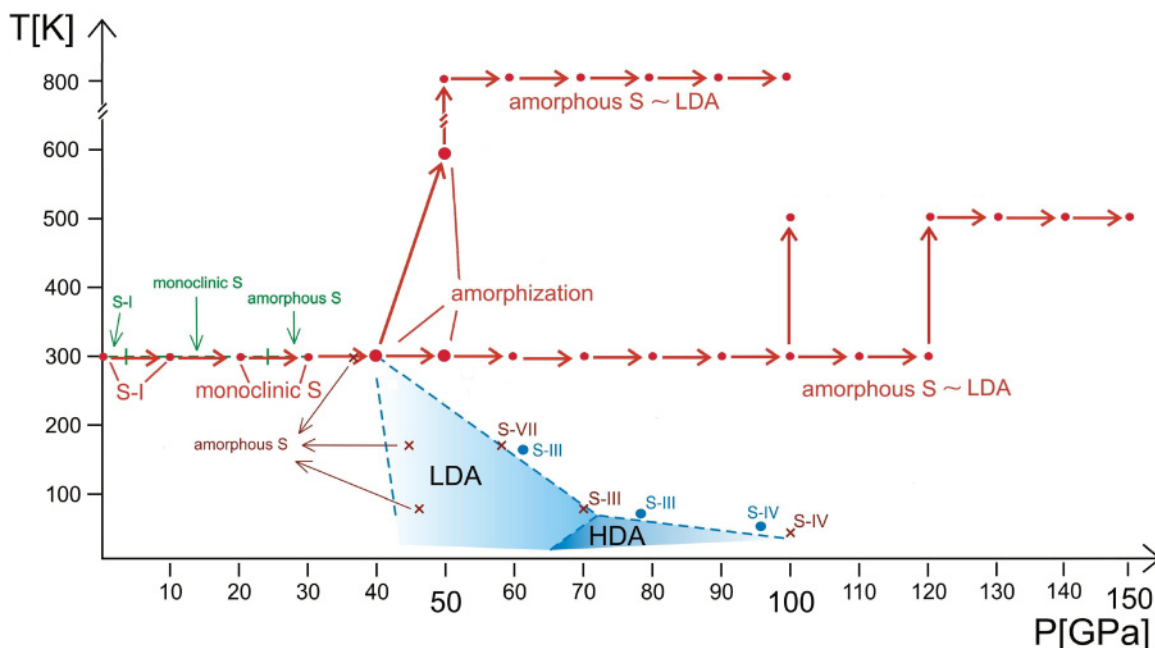


FIG. 2. (Color online) Simulation protocol of the present study (red dots and arrows) along experimental data for amorphous sulfur from Ref. 18 (green), Ref. 20 (brown) and Refs. 15 and 19 (LDA and HDA forms in light and dark blue). Three amorphization points are marked by bold circles.

structure at 0 GPa and 0 K and initially heated the system at zero pressure to 300 K. Afterward, we gradually increased pressure in 10 GPa steps keeping the temperature at 300 K. We allowed the system to equilibrate for 4 ps at pressures up to 30 GPa and for 10–30 ps at higher pressures where substantial structural changes take place. At 20 GPa we observed a transition to a new molecular phase with monoclinic lattice formed by S_8 molecules with two different conformations. Upon further increase of pressure to 40 GPa we observed initial creation of structural defects in molecular structure where few bond interchanges between nearby molecules were present. From this point, we proceeded with simulation along three different paths. We extended the 40 GPa simulation up to nearly 30 ps, which gave us access to detailed information about early stages of PIA. Second, after 4 ps run at 40 GPa, we increased pressure to 50 GPa and beyond, keeping the system at room temperature. Third, we increased both pressure to 50 GPa and temperature to 600 K in order to further accelerate PIA. PIA in our simulations was, therefore, observed at three different P-T conditions. The amorphous states created at 50 GPa thereafter persisted to very high P-T points (150 GPa, 500 K) and (100 GPa, 800 K) with no sign of progress in recrystallization or transition to different amorphous form (Fig. 2).

In the following subsections we discuss in detail the properties of the monoclinic phase, analyze the origin and dynamics of the PIA transformation, and study the properties of the amorphous form. We shall denote the monoclinic and amorphous forms found in our simulations as m-S and a-S.

B. Monoclinic sulfur

As we increased pressure from 10 to 20 GPa, the supercell of S-I distorted by lowering the α angle from 90° to 86.5° at 40 GPa according to MD simulations at 300 K and subsequent geometric optimization at zero temperature. This change of supercell is compatible with change of lattice symmetry from orthorhombic to monoclinic. At the same time, half of the originally identical S_8 molecules deformed to less symmetric form. We denote these deformed S_8 molecules in m-S as type B and the original ones as type A.

Type A molecules are naturally most common 8-atomic ring-puckered D_{4d} isomer with crown shape.^{21,58,59} This isomer forms α , β , and γ -S structures and is also present in liquid sulfur. Type B molecules originated from deformation of type A molecules and possess lower C_2 symmetry. Their shape is shown and compared to the D_{4d} isomer in Fig. 3 together with the schematic view on the structure of m-S.

As far as m-S appears to be a new structure of sulfur, we optimized the 128 atom cell representing quarter of the simulation supercell.⁶¹ The relation of m-S to monoclinic-S found by Luo and Ruoff could not be determined because structural data for this phase are not available. We were not able to find the exact space group symmetry for this complex monoclinic phase with large unit cell.

We also calculated the equation of states (EOS) of S-I and m-S to compare their relative stability. According to the calculated EOS, we found that m-S at zero temperature is more stable than S-I at pressures greater than 29 GPa. We also found that optimization of the m-S unit cell at 50 GPa and higher

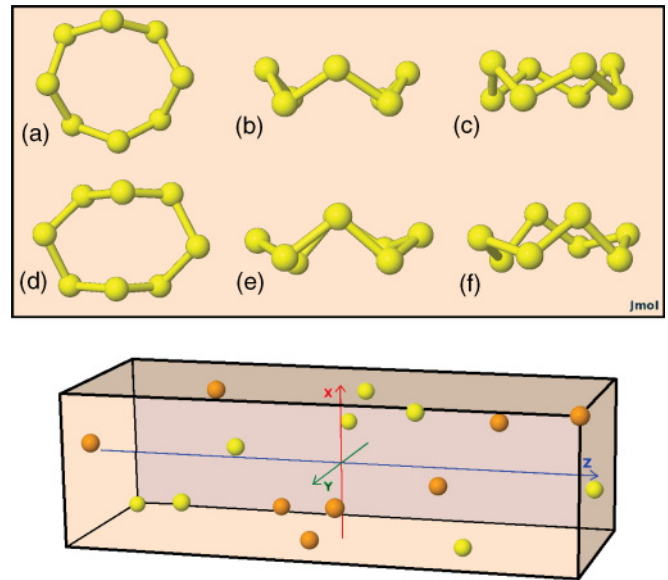


FIG. 3. (Color online) Comparison of type A (a)–(c) and type B (d)–(f) molecules and visualization of m-S structure. Yellow (lighter) spheres represent mass centers of original type A molecules and orange (darker) spheres represent centers of deformed type B molecules. Pictures were generated by Jmol.⁶⁰

pressures resulted into formation of amorphous form directly during structural optimization. This leads to the conclusion that 50 GPa is the upper limit of the metastability of molecular m-S structure and beyond 50 GPa m-S cannot exist anymore.

C. Mechanism and dynamics of pressure-induced amorphization

The 30 ps simulation run at 40 GPa gives us access to detailed information about the early stages of PIA. On Fig. 4 we show the evolution of the system density from the beginning of compression (at 0 ps) from 30 to 40 GPa till the end of the 40 GPa run. In this figure, the elastic and nonelastic parts of the density increase can be clearly recognized. The increase of density from 3.63 to 3.94 g cm^{-3} at 1.5 ps corresponds to the elastic compression of molecular m-S. At 1.5 ps, the pressure in the system is equilibrated to external 40 GPa, and the m-S structure in next 6.5 ps does not undergo any change. At 8 ps, however, the system spontaneously starts to amorphize and one can see a step-wise increase in density persisting until 21 ps of the MD run. Densification during amorphization is accompanied by further decrease of the monoclinic angle from 86.5° to 83.2° in a-S at the end of the MD run. The resulting amorphous version of sulfur at 40 GPa has density of 4.04 g cm^{-3} that corresponds to density increase of 2.54% from m-S at 40 GPa. It is plausible to assume that the compression would further continue if longer simulation times were accessible. Amorphous versions of sulfur obtained at pressure of 50 GPa and temperatures of 300 and 600 K were investigated to much higher pressures (to 150 GPa in lower and to 100 GPa in higher temperature branch). We did not observe any significant jump in density that could be associated with the LDA to HDA polyamorphic transition. The graph of densities of sulfur from 10 to 150 GPa together with the data from Refs. 15 and 19 is

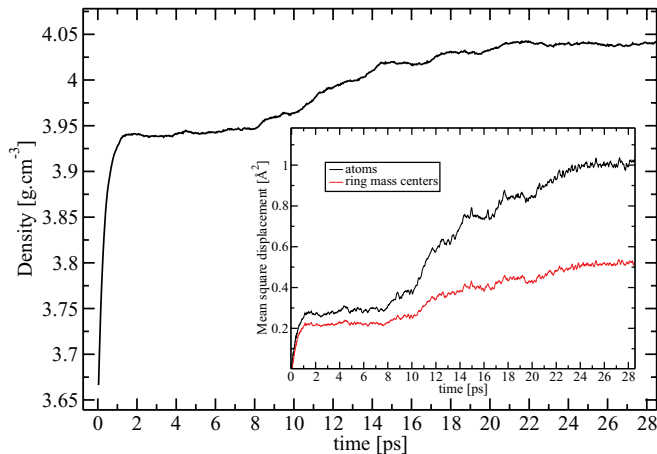


FIG. 4. (Color online) Density relaxation during m-S \rightarrow a-S transition at 40 GPa. Elastic compression of m-S completed in 1.5 ps is followed by 6.5 ps run when m-S remains crystalline. At 8 ps the amorphization starts and in the following 13 ps the system undergoes non-elastic densification. (Inset) Mean square displacement $\Delta r^2(t)$ as a function of time for atoms (upper black curve) and ring mass centers (lower red curve) for the entire MD run at 40 GPa. The MSD curves have clearly distinct character in the crystalline m-S, where MSD stabilizes at constant value until amorphization begins at 8 ps, and after 8 ps, where it starts to grow rapidly. The curves of the MSD still grow till the end of the run which means that the amorphization process is not yet completed and further density increase could be expected if considerably longer simulation times were available.

shown in Fig. 5. Together with the increase of density, the process of amorphization between 8 and 21 ps leads into an increase of average energy while enthalpy decreases by 30 meV per particle.

Since during the amorphization transformation the atoms are likely to diffuse over finite distances away from their original positions in the crystalline phase, we computed the time-dependent mean-square displacement $\Delta r^2(t)$ (MSD) of

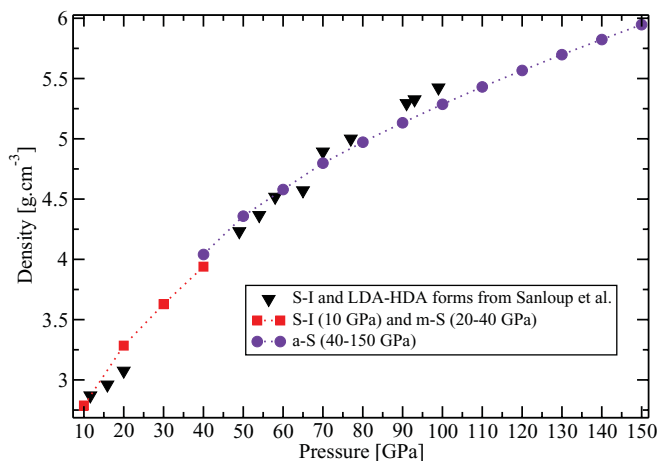


FIG. 5. (Color online) Density of sulfur under pressure according to the presented MD simulations (red squares for m-S and violet circles for a-S) and S-I and LDA-HDA densities from Refs. 15 and 19 (black triangles). Our results are for 300 K for pressures 10–120 GPa and for 500 K for 130–150 GPa. The transition from m-S to a-S at 40 GPa is seen as a small jump in density.

atoms and molecular mass-centers in order to monitor the diffusion during amorphization. The values of $\Delta r^2(t)$ are evaluated as

$$\Delta r^2(t) = \frac{1}{N} \sum_{i=1}^N (\mathbf{r}_i(t) - \mathbf{r}_i(0))^2,$$

where $\mathbf{r}_i(0)$ are the initial positions which are subtracted from the actual ones $\mathbf{r}_i(t)$ at every time step. We have plotted the time-dependent MSD of atoms and mass-centers for m-S and a-S at 40 GPa in the inset of Fig. 4. From the graph, one can see a clear difference between the character of MSD in crystalline and amorphous sulfur in the time interval where both phases exist. The crystalline case is recognized by a constant value of MSD between 1.5 and 8 ps, while during the amorphization, MSD of atoms and mass-centers grows even after 28 ps. This shows that despite volume stabilization at 21 ps, the structure continues to evolve as amorphization proceeds. This also points to the intrinsic time-scale limitation of the *ab initio* study since following the evolution of this fairly large system over substantially longer time, although very desirable, would be prohibitively expensive.

In molecular crystals at low pressure, the intermolecular distances between atoms are typically much larger than the corresponding intramolecular ones. Upon compression the former ones decrease as the molecules approach each other and when the two kinds of distances become comparable a transition from molecular to nonmolecular, or polymeric phase, may take place. Examples are N_2 ,⁶² CO_2 ,⁶³ etc. It is plausible to assume that a similar scenario may apply here. In particular, the PIA of the strongly overpressurized ring-molecular phase could be triggered as the molecules approach each other closely.

In order to check this possibility we focused on the evolution of intramolecular bond lengths and intermolecular distances upon increasing pressure. Compression of m-S leads to considerable decrease in intermolecular space, while the intramolecular bond lengths remain practically unchanged. We also observed a lowering of the bond angles in molecules from 107° at 10 GPa to 97° at 40 GPa.

In Fig. 6 we present the distributions of the nearest neighbors (n.n.) intramolecular distances (bond lengths) and the nearest intermolecular distances in S-I and m-S at pressures from 10 to 40 GPa. Every molecule contributes with eight values to both histograms and the nearest intermolecular distance is defined as the closest distance between the atom and all atoms in other molecules.

We see that up to the pressure of 30 GPa the two distributions are clearly separated and do not overlap. Under these conditions the molecular phase persists. At 40 GPa, we see that the intermolecular distribution develops a small peak located around the sulfur bond length. This points to the existence of structural defects in m-S where certain atoms from different molecules start bonding.

Even without existence of defects, the figure reveals that at 40 GPa molecules interact strongly as their intra and intermolecular distances distributions start to overlap. We note that in experiment at room temperature the PIA was observed at 37 GPa,²⁰ which is in perfect agreement with our results. The data suggest that PIA is likely to be primarily driven by

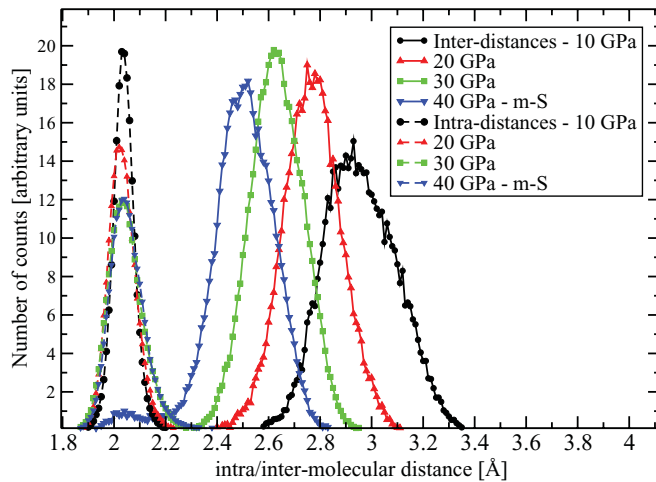


FIG. 6. (Color online) Comparison of bond length and nearest intermolecular distance distributions in S-I at 10 GPa and in m-S at 20–40 GPa. The structure of m-S becomes unstable at 40 GPa where the distributions start to overlap. The structure of m-S at 40 GPa contains some bonds between different molecules (defects) that are represented by the small peak around the sulfur covalent diameter of 2.04 Å. The distribution at 40 GPa is averaged over 6.5 ps interval of m-S existence.

the overlap of these two distributions, similarly to other cases of molecular to non-molecular transformation in crystals.

This scenario is further confirmed by analyzing the dynamics of the early stages of the PIA. We show in Fig. 7 the evolution of the nearest intermolecular distances histograms averaged over short time intervals at 12, 15, and at 27 ps of the 40 GPa run. As presented in the figure, the character of the nearest intermolecular distance distribution considerably changes at 12 ps when it develops a major peak weighted around the sulfur bond length. At the end of the 40 GPa run, many of the atoms are already forming covalent bonds with

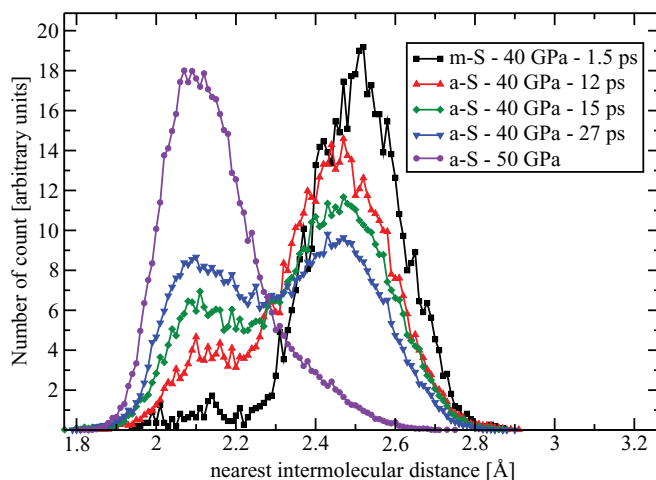


FIG. 7. (Color online) Evolution of the nearest intermolecular distance distribution during amorphization at 40 GPa. Starting from the defective m-S at 1.5 ps, the histogram moves left as more and more atoms make their bonds with surrounding molecules. Distribution at 50 GPa, where most of the atoms bond to other molecules, is shown for comparison.

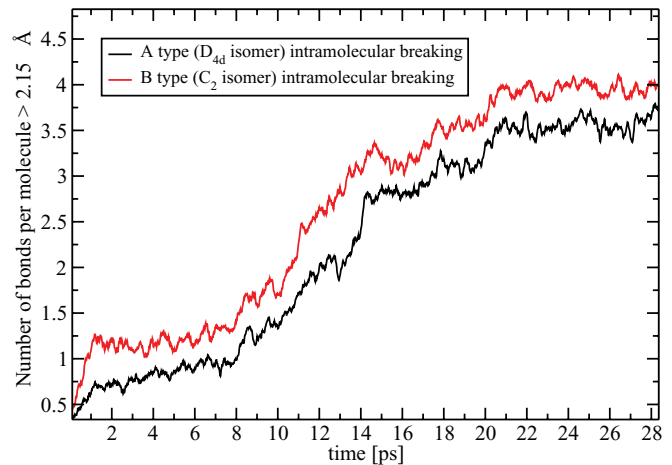


FIG. 8. (Color online) Number of intramolecular distances longer than 2.15 Å in type A molecules (D_{4d} isomer) and in type B molecules (C_2 isomer). The numbers are normalized such that they represent an average number of bonds longer than the limit per one molecule of certain type. Amorphization at 40 GPa starting at 8 ps is represented by rapid growth of both curves as intramolecular bonds are progressively broken. At the end of the run, roughly half of the bonds in molecules is broken.

atoms from different—previously separated molecules. By visual inspection we also find that the amorphization process proceeds mainly around the original structural defects.

In order to further clarify the amorphization transformation, we also study the interactions between type A and type B molecules separately. In Fig. 8 we show the evolution of the number of intramolecular distances longer than 2.15 Å for A and B molecules. (This limit has been conventionally chosen and is 5.4% longer than sulfur covalent diameter 2.04 Å). The number of bond lengths longer than 2.15 Å in type B molecules is always somewhat greater than in A molecules, indicating that type B molecules are more likely to develop bond breakings than A molecules.

As a complementary information to bond lengths evolution, on Fig. 9 we investigate the number of intermolecular distances shorter than 2.2 Å (close intermolecular approachings) for A-A, B-B, and A-B pairs separately. The figure confirms that B molecules are indeed more involved in the early stages of amorphization, which starts by a sudden increase of the number of the B-B approachings at 8 ps. Only after the next two picoseconds, molecules A and B start to mix together as the A-B curve starts to grow after 10 ps. The mixing of A molecules starts even later, 3 ps after the beginning of A-B mixing. At the end of the run at 40 GPa, approximately 30% of all atoms have one atom from a different molecule closer than 2.2 Å, on average. This clearly shows that the amorphization at 40 GPa proceeds slowly and even after 30 ps we still observe early stages of the process.

Altogether, the analysis of bond lengths and intermolecular distances evolution during amorphization provides interesting information about the ring disintegration process leading to amorphization. In particular, we identify the different role played by the A and B molecules.

In order to further characterize the transition from crystalline to disordered structure, we also note that the mean

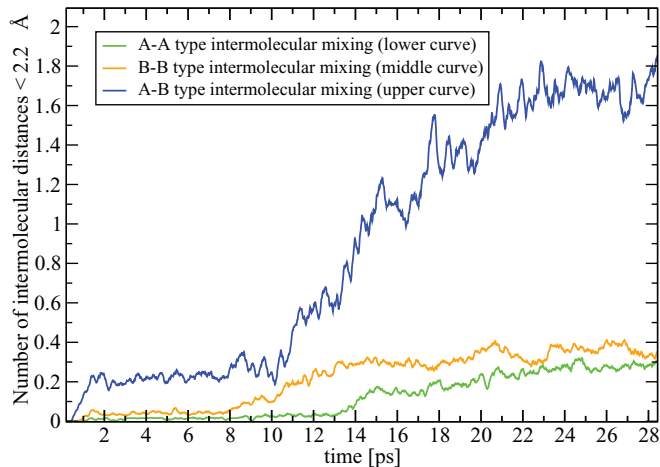


FIG. 9. (Color online) Number of intermolecular distances shorter than 2.2 \AA between type A molecules (lower green curve), between type B molecules (middle orange curve) and between A-B molecules mixed (upper blue curve). Amorphization starting at 8 ps corresponds to the first increase of the B-B curve followed by rapid A-B mixing starting at 10 ps and mixing between A molecules that starts another 3 ps later. The normalization is chosen such that the sum of all three graphs represents an average number of the intermolecular distances shorter than 2.2 \AA per one molecule. (Note that there are more than twice as many possible connections for A-B pairs than for A-A and B-B pairs.)

intramolecular distance between previously identified n.n. grew from 2.06 \AA in m-S at 40 GPa to 2.60 \AA in a-S at 50 GPa. Although this quantity no longer represents any kind of bond length, it provides information about the amount of diffusion in the system, in addition to the previously shown time-dependent MSD.

D. Amorphous form

S-I at ambient pressure is a soft material with $\beta = 7.7 \text{ GPa}$. This reflects the presence of fairly large intermolecular space. The crystal to amorphous form transition at 40 GPa is accompanied by sharp increase of density (Figs. 4 and 5) possibly indicating the first-order nature of the transition as suggested in Ref. 19.

After obtaining a-S at 50 GPa, we performed further simulations at higher pressures and also at higher temperatures (Fig. 2). Even at the highest pressure of 150 GPa and elevated temperature of 800 K at 100 GPa we have not found any evidence of recrystallization or transition to a distinct amorphous form. On the contrary, we have found a-S created at 50 GPa to remain without any serious change of structure, except for slow equilibration of the first peak of the radial distribution function (RDF) of a-S, as will be discussed later. The lack of observation of recrystallization was most likely caused by short time scale of our simulations. In principle, the nonobservation of transition to HDA form, if this indeed exists, could be related to the same time scale problem.

In Fig. 10, we present the RDFs of m-S at 40 GPa and a-S at 40, 50, and 70 GPa. The decrease of the first peak maximum and the filling of the first minimum is a consequence of breaking of intramolecular bonds. As molecules start to

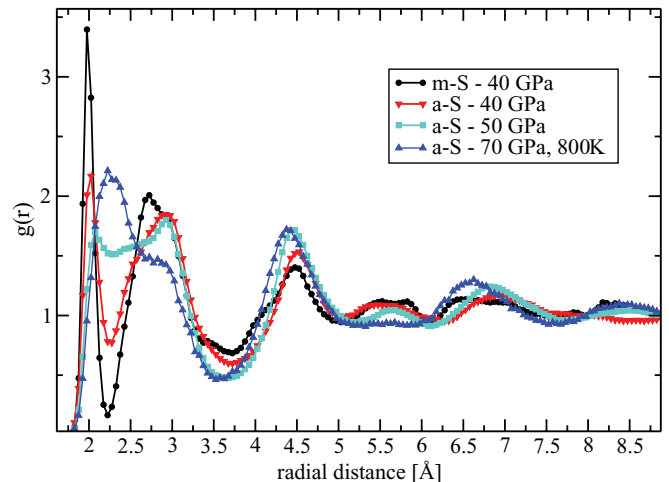


FIG. 10. (Color online) Comparison of RDFs of m-S at 40 GPa (black circled curve) and a-S at 40 GPa (red down triangles), at 50 GPa (turquoise squares), and at 70 GPa and 800 K (blue up triangles). Similarity of RDFs at 40 GPa reflects close relation of 40 GPa a-S to m-S. RDF of a-S at 70 GPa corresponds quite well to the experimental $g(r)$ in Ref. 19 even though simulated $g(r)$ is not fully equilibrated.

disintegrate and make more bonds with other molecules, the first two peaks start merging, although second peak remains recognizable even to highest P-T conditions investigated in our simulations. This persisting first peak separation indicates that some short-range order of m-S remains present during simulated PIA, since there is still some abundance of the next-to-n.n. distances. This implies that our a-S still contains some fragments of the original S_8 molecules.

Next, we analyze the properties of a-S and its correspondence to the LDA form from Ref. 19. We find that a-S and LDA are indeed very similar, but the possible relation of a-S to some underlying crystalline phase could not be clearly identified.

First, we observe that the RDF of a-S corresponds quite well to the RDF of LDA from Ref. 19. We refer to the resemblance between the RDF of LDA at 65 GPa (Ref. 19) and the RDF of a-S at 70 GPa shown as blue up triangles in Fig. 10. The agreement of the densities between a-S and LDA is also very good, especially at 60 GPa (see Fig. 5).

Next, we find that the value of the coordination number in a-S at 50 GPa is $N_C = 16.2$ (for $r_c = 3.65 \text{ \AA}$) and $N_C = 16.1$ at 70 GPa ($r_c = 3.5 \text{ \AA}$), which is again in close agreement with the experimental value of 16.1 at 65 GPa from Ref. 19. This suggests that our a-S is indeed similar to the experimentally observed LDA form.

Now, we discuss the suggestion put forward in Ref. 19, namely that the LDA form might be structurally related to crystal phase S-III. This suggestion was based on the comparison of density and coordination number, which is 17 in S-III for the same r_c radius as for LDA. This relation also seems plausible taking into account the positions of the two forms in the phase diagram.

While N_C in the S-III phase calculated to the first LDA minimum is 17, we found that N_C for m-S at 40 GPa with cutoff $r_c = 3.8 \text{ \AA}$ (which is the first minimum of a-S at 40 GPa), equals 15.9. We note that in the case of m-S, the distance of

3.8 Å naturally corresponds to the second RDF minimum at 40 GPa. Therefore, the simulated a-S could also be structurally related to its parent phase m-S, rather than to S-III.

Change of the structure of sulfur under pressure is also accompanied by change of its electronic properties. We found that the amorphization at 40 and 50 GPa is also accompanied by metallization. According to the computed electronic density of states (eDOS), we found m-S to be an insulator up to 30 GPa with energy band gap of 0.4 eV at 20 GPa and 0.1 eV at 30 GPa. At 40 GPa, we found a small elevation of the eDOS minimum at Fermi energy to a nonzero value before amorphization of m-S started. In the case of a-S at 40 GPa and at higher pressures, we find the amorphous form to be metallic. Due to the well-known problem of underestimation of energy gap in DFT calculations using approximate exchange-correlation functionals it is possible that the true gaps in respective phases might be larger.

IV. CONCLUSIONS

We performed *ab initio* constant-pressure MD simulations of elemental sulfur on a sample containing 512 atoms. We observed two transitions: from S-I to m-S at 20 GPa and from m-S to a-S at 40 and 50 GPa. The structure of m-S is similar to S-I and might correspond to monoclinic-S observed by Luo and Ruoff in Ref. 18. It consists of distorted (called

type B) and undistorted (type A) S₈ molecules. While the a-S form we found appears rather similar to the experimentally found LDA form from Ref. 19, we did not find a subsequent transition to HDA form. This could either reflect a too-short time scale of our simulations or the possibility put forward in Ref. 19 that the observed LDA and HDA forms might actually have nanocrystalline structure. The possible relation of a-S to underlying crystal phase is not clear, since we found similarities to both m-S and S-III. The density-driven amorphization process starts at 40 GPa when the distributions of nearest intra and intermolecular distances begin to overlap. This leads to bond interchanges and eventually to molecular disintegration and formation of structurally disordered phase. We found that in the early stages of the amorphization process, the B molecules are substantially more involved than A molecules. It would be interesting to obtain, if possible, high-quality diffraction pattern for the crystalline structure before PIA and compare it to our m-S.

ACKNOWLEDGMENTS

This work was supported by the Slovak Research and Development Agency under Contract No. APVV-0558-10 and by the project implementation 26220220004 within the Research & Development Operational Programme funded by the ERDF.

*dusan.plasienska@fmph.uniba.sk

¹O. Mishima, L. D. Calvert, and E. Whalley, *Nature (London)* **310**, 939 (1984).
²S. K. Deb, M. Wilding, M. Somayazulu, and P. F. McMillan, *Nature (London)* **414**, 528 (2001).
³R. J. Hemley, A. P. Jephcoat, H. K. Mao, L. C. Ming, and M. H. Manghnani, *Nature (London)* **334**, 52 (1988).
⁴A. K. Arora, in *High Pressure Phenomena*, edited by R. J. Hemley and G. L. Chiarotti (IOS Press, Amsterdam, The Netherlands, 2002), pp. 545–560.
⁵S. M. Sharma and S. K. Sikka, *Prog. Mat. Sci.* **40**, 1 (1996).
⁶N. Binggeli and J. R. Chelikowsky, *Phys. Rev. Lett.* **69**, 2220 (1992).
⁷V. V. Brazhkin, A. Lyapin, O. Stalgorova, E. Gromnitskaya, S. Popova, and O. Tsiok, *J. Non-cryst. Solids* **212**, 49 (1997).
⁸O. Mishima, L. D. Calvert, and E. Whalley, *Nature (London)* **314**, 76 (1985).
⁹D. Daisenberger, M. Wilson, P. F. McMillan, R. Quesada Cabrera, M. C. Wilding, and D. Machon, *Phys. Rev. B* **75**, 224118 (2007).
¹⁰E. Principi, A. DiCiccio, F. Decremps, A. Polian, S. DePanfilis, and A. Filippini, *Phys. Rev. B* **69**, 201201 (2004).
¹¹L. Huang and J. Kieffer, *Phys. Rev. B* **69**, 224203 (2004).
¹²K. Trachenko and M. T. Dove, *Phys. Rev. B* **67**, 212203 (2003).
¹³M. Durandurdu and D. A. Drabold, *Phys. Rev. B* **65**, 104208 (2002).
¹⁴K. Trachenko, M. T. Dove, V. Brazhkin, and F. S. El'kin, *Phys. Rev. Lett.* **93**, 135502 (2004).
¹⁵C. Sanloup, in *High-Pressure Crystallography: From Fundamental Phenomena to Technological Applications*, edited by E. Boldyreva and P. Dera (Springer, Dordrecht, The Netherlands, 2010), chap. 37, pp. 459–468.

¹⁶P. F. McMillan, *J. Mat. Chem.* **14**, 1506 (2004).

¹⁷P. F. McMillan, in *High Pressure Phenomena*, edited by R. J. Hemley and G. L. Chiarotti (IOS Press, Amsterdam, The Netherlands, 2002), pp. 511–541.
¹⁸H. Luo and A. L. Ruoff, *Phys. Rev. B* **48**, 569 (1993).
¹⁹C. Sanloup, E. Gregoryanz, O. Degtyareva, and M. Hanfland, *Phys. Rev. Lett.* **100**, 075701 (2008).
²⁰E. Gregoryanz (private communication).
²¹B. Meyer, *Chemical Reviews* **76**, 367 (1976).
²²O. Degtyareva, E. Gregoryanz, M. Somayazulu, P. Dera, H. K. Mao, and R. Hemley, *Nat. Mater.* **4**, 152 (2005).
²³O. Degtyareva, E. Hernández, J. Serrano, M. Somayazulu, H. K. Mao, E. Gregoryanz, and R. Hemley, *J. Chem. Phys.* **126**, 084503 (2007).
²⁴O. Degtyareva, E. Gregoryanz, M. Somayazulu, H. K. Mao, and R. J. Hemley, *Phys. Rev. B* **71**, 214104 (2005).
²⁵O. Degtyareva, M. V. Magnitskaya, J. Kohanoff, G. Profeta, S. Scandolo, M. Hanfland, M. I. McMahon, and E. Gregoryanz, *Phys. Rev. Lett.* **99**, 155505 (2007).
²⁶O. Degtyareva, E. Gregoryanz, H. K. Mao, and R. J. Hemley, *High Press. Res.* **25**, 17 (2005).
²⁷C. Hejny, L. F. Lundegaard, S. Falconi, M. I. McMahon, and M. Hanfland, *Phys. Rev. B* **71**, 020101 (2005).
²⁸L. Crapanzano, W. A. Crichton, G. Monaco, R. Bellissent, and M. Mezouar, *Nat. Mater.* **4**, 550 (2005).
²⁹O. Zakharov and M. L. Cohen, *Phys. Rev. B* **52**, 12572 (1995).
³⁰A. R. Oganov and C. W. Glass, *J. Chem. Phys.* **124**, 244704 (2006).
³¹C. Pastorino and Z. Gamba, *J. Chem. Phys.* **119**, 2147 (2003).
³²S. P. Rudin and A. Y. Liu, *Phys. Rev. Lett.* **83**, 3049 (1999).

- ³³H. Fujihisa, Y. Akahama, H. Kawamura, H. Yamawaki, M. Sakashita, T. Yamada, K. Honda, and T. LeBihan, *Phys. Rev. B* **70**, 134106 (2004).
- ³⁴A. Nishikawa, *J. Phys.: Conf. Ser.* **121**, 012008 (2008).
- ³⁵H. Luo, R. G. Greene, and A. L. Ruoff, *Phys. Rev. Lett.* **71**, 2943 (1993).
- ³⁶A. Nishikawa, K. Niizeki, and K. Shindo, *Phys. Status Solidi B* **211**, 373 (1999).
- ³⁷H. Luo, S. Desgreniers, Y. K. Vohra, and A. L. Ruoff, *Phys. Rev. Lett.* **67**, 2998 (1991).
- ³⁸K. J. Dunn and F. P. Bundy, *J. Chem. Phys.* **67**, 5048 (1977).
- ³⁹E. Gregoryanz, V. V. Struzhkin, R. J. Hemley, M. I. Erements, H. K. Mao, and Y. A. Timofeev, *Phys. Rev. B* **65**, 064504 (2002).
- ⁴⁰R. Bellissent, L. Descotes, F. Boué, and P. Pfeuty, *Phys. Rev. B* **41**, 2135 (1990).
- ⁴¹A. G. Kalampounias, K. S. Andrikopoulos, and S. N. Yannopoulos, *J. Chem. Phys.* **118**, 8460 (2003).
- ⁴²T. Scopigno, S. N. Yannopoulos, F. Scarponi, K. S. Andrikopoulos, D. Fioretto, and G. Ruocco, *Phys. Rev. Lett.* **99**, 025701 (2007).
- ⁴³G. Monaco, L. Crapanzano, R. Bellissent, W. Crichton, D. Fioretto, M. Mezouar, F. Scarponi, and R. Verbeni, *Phys. Rev. Lett.* **95**, 255502 (2005).
- ⁴⁴M. Springborg and R. O. Jones, *Phys. Rev. Lett.* **57**, 1145 (1986).
- ⁴⁵J. S. Tse and D. D. Klug, *Phys. Rev. B* **59**, 34 (1999).
- ⁴⁶R. O. Jones and P. Ballone, in *Third International Conference: Computational Modeling and Simulation of Materials - Part A*, edited by P. Vincenzini and A. Lami (Techna Group Srl, Faenza, Italy, 2004), pp. 281–288.
- ⁴⁷P. Yu, W. H. Wang, R. J. Wang, S. X. Lin, X. R. Liu, S. M. Hong, and H. Y. Bai, *Appl. Phys. Lett.* **94**, 011910 (2009).
- ⁴⁸Y. Akahama, M. Kobayashi, and H. Kawamura, *Phys. Rev. B* **48**, 6862 (1993).
- ⁴⁹G. Kresse and J. Furthmüller, *Phys. Rev. B* **54**, 11169 (1996).
- ⁵⁰G. Kresse and J. Furthmüller, *Comput. Mater. Sci.* **6**, 15 (1996).
- ⁵¹G. Kresse and J. Hafner, *Phys. Rev. B* **47**, 558 (1993).
- ⁵²G. Kresse and J. Hafner, *Phys. Rev. B* **49**, 14251 (1994).
- ⁵³H. J. C. Berendsen, J. P. M. Postma, W. F. van Gunsteren, A. DiNola, and J. R. Haak, *J. Chem. Phys.* **81**, 3684 (1984).
- ⁵⁴P. E. Blöchl, *Phys. Rev. B* **50**, 17953 (1994).
- ⁵⁵G. Kresse and D. Joubert, *Phys. Rev. B* **59**, 1758 (1999).
- ⁵⁶J. P. Perdew, K. Burke, and M. Ernzerhof, *Phys. Rev. Lett.* **77**, 3865 (1996).
- ⁵⁷W. Kohn and L. J. Sham, *Phys. Rev.* **140**, 1133 (1965).
- ⁵⁸R. O. Jones and P. Ballone, *J. Chem. Phys.* **118**, 9257 (2003).
- ⁵⁹D. Hohl, R. O. Jones, R. Car, and M. Parrinello, *J. Chem. Phys.* **89**, 6823 (1988).
- ⁶⁰Jmol: An open-source java viewer for chemical structures in 3D: [<http://www.jmol.org/>].
- ⁶¹See Supplemental Material at <http://link.aps.org/supplemental/10.1103/PhysRevB.85.094112> for the atomic coordinates of the optimized m-S structure at 20 GPa (in .xyz format).
- ⁶²A. F. Goncharov, E. Gregoryanz, H. K. Mao, Z. Liu, and R. J. Hemley, *Phys. Rev. Lett.* **85**, 1262 (2000).
- ⁶³M. Santoro, F. A. Gorelli, R. Bini, G. Ruocco, S. Scandolo, and W. A. Crichton, *Nature (London)* **441**, 857 (2006).